Structural basis for complement factor H–linked age-related macular degeneration

Beverly E. Prosser,[1] Steven Johnson,[1] Pietro Roversi,[1] Andrew P. Herbert,[3] Bärbel S. Blaum,[3] Jess Tyrrell,[1] Thomas A. Jowitt,[4] Simon J. Clark,[2,4] Edward Tarelli,[5] Dušan Uhrín,[3] Paul N. Barlow,[3] Robert B. Sim,[2] Anthony J. Day,[2,4] and Susan M. Lea[1]

[1]Sir William Dunn School of Pathology and the [2]Medical Research Council Immunochemistry Unit, Department of Biochemistry, University of Oxford, Oxford, OX1 3RE, England, UK
[3]Joseph Black Chemistry Building, University of Edinburgh, Edinburgh, EH9 3JJ, Scotland, UK
[4]Wellcome Trust Centre for Cell-Matrix Research, University of Manchester, Manchester M13 9PT, England, UK
[5]Medical Biomics Centre, St. George's University of London, London SW17 0RE, England, UK

Nearly 50 million people worldwide suffer from age-related macular degeneration (AMD), which causes severe loss of central vision. A single-nucleotide polymorphism in the gene for the complement regulator factor H (FH), which causes a Tyr-to-His substitution at position 402, is linked to ~50% of attributable risks for AMD. We present the crystal structure of the region of FH containing the polymorphic amino acid His402 in complex with an analogue of the glycosaminoglycans (GAGs) that localize the complement regulator on the cell surface. The structure demonstrates direct coordination of ligand by the disease-associated polymorphic residue, providing a molecular explanation of the genetic observation. This glycan-binding site occupies the center of an extended interaction groove on the regulator's surface, implying multivalent binding of sulfated GAGs. This finding is confirmed by structure-based site-directed mutagenesis, nuclear magnetic resonance–monitored binding experiments performed for both H402 and Y402 variants with this and another model GAG, and analysis of an extended GAG–FH complex.

CORRESPONDENCE
Susan M. Lea:
susan.lea@path.ox.ac.uk
OR
Anthony J. Day:
anthony.day@manchester.ac.uk

Abbreviations used: AMD, age-related macular degeneration; CCP, complement control protein module; CRP, C-reactive protein; FH, factor H; GAG, glycosaminoglycan; NMR, nuclear magnetic resonance; SCR, short consensus repeat domain; SOS, sucrose octasulfate.

Age-related macular degeneration (AMD) is the major cause of irreversible blindness in the elderly population of the developed world (1). The disease is characterized by loss of central vision, which is caused by progressive deterioration of the macula, with symptoms presenting in old age. A significant risk factor for development of the disease has recently been demonstrated to be a common allelic variant of complement factor H (FH) (2–5), resulting in a tyrosine/histidine polymorphism at position 402 (384 in the mature protein) (6). Individuals heterozygous for the His-form are 2.7-fold more likely to develop AMD (50% of the attributable risk factors) (4), whereas risk of AMD increases by >7.4-fold for His402 homozygotes (2). The physiological role of FH, which consists of 20 short consensus repeat (SCR) or complement control protein (CCP) modules (7), is to regulate complement by accelerating the decay of the alternative pathway C3 convertase and by acting as a cofactor for factor I–mediated proteolysis of C3b (8–10). It is capable of complement regulation in both the fluid phase and on the surface of cells, where it is localized via binding to cell surface polyanions (11), such as sialic acid and glycosaminoglycan (GAG) chains of proteoglycans. Specific polyanion binding has been definitively mapped to SCR20 at the C terminus of FH (12), and also to SCR7 (13), which contains the polymorphic residue 402. Sites in other SCRs have been proposed, but no final consensus has been reached on their possible physiological relevance (14, 15). In addition, FH has been shown to bind C-reactive protein (CRP), also via SCR7, thereby contributing to noninflammatory phagocytosis of damaged tissue (16).

The late onset of AMD implies that any alterations in natural function caused by the polymorphism are likely to be subtle, and may be linked to age-related alterations of retinal GAG composition (17, 18). It has been observed that the relative affinities of the two polymorphs for subtly different ligands vary greatly (18–21). Collectively, the current data imply that the FH

B.E. Prosser and S. Johnson contributed equally to this paper.
The online version of this article contains supplemental material.

Tyr402His polymorphism alters the precise specificity and affinity of its interaction with GAGs and CRP on the cell surface, leading to altered levels of FH retention on the retinal/macular surface, and thereby affecting complement activity in the area. NMR structures of SCR7s from both polymorphs (19) have demonstrated that their structures are identical, including the orientation of the altered sidechain. To gain insight into the functional consequences of the Y402H polymorphism, we have determined the crystal structure at 2.35 Å of the H402 variant of a three-domain region of FH surrounding the site of AMD-associated polymorphism (FH SCR6–8; hereafter termed FH-678$_{402H}$) in complex with sucrose octasulfate (SOS), which is a highly sulfated sugar analogue of GAGs. To validate the SOS interactions to more physiologically relevant GAG interactions, we have performed NMR-monitored titrations using His402 and Tyr402 versions of various FH constructs, and of both SOS and a highly sulfated heparin tetrasaccharide. These experiments (Fig. S1, available at http://www.jem.org/cgi/content/full/jem.20071069/DC1) demonstrate that both of these sulfated analogues of natural GAGs have identical binding modes and validate our selection of SOS for the crystallographic studies of FH–GAG binding.

RESULTS AND DISCUSSION

Crystallographic structure of FH modules 6–8 in complex with SOS

The inherently flexible nature of the 20-module-long FH renders it a difficult target for atomic resolution structure determination. Therefore, we designed constructs containing the disease-implicated SCR7 flanked on either side by a single SCR module (SCR6 and 8). Both histidine and tyrosine polymorphs were characterized for their different GAG interaction characteristics (18), and both were shown to exhibit subtly different GAG-binding specificities (Fig S2, available at http://www.jem.org/cgi/content/full/jem.20071069/DC1) (18). Crystallization trials with both variants with and without a sugar ligand (SOS) were performed (22); however, only the combination of the His402 construct with a 10-fold molar excess of SOS yielded crystals. NMR was used to check that another model GAG (a highly sulfated heparin-derived tetrasaccharide) binds in a similar way to SOS. The structure was solved using a combination of molecular replacement (with the NMR structure for SCR7 [reference 19]) and experimental phases (see Materials and methods and Supplemental materials and methods). The FH678$_{402H}$ structure (Fig. 1 A and Table I) adopts an extended, but slightly curved, conformation, with a tight interface between SCR6 and 7, and weaker interactions between SCR7 and 8. SOS is seen to mediate the vast majority of crystal contacts, explaining the observation that crystallization only occurred in the presence of SOS (22). The NMR and crystal structures of FH7$_{402H}$ are identical, showing that the His402 sidechain adopts the same conformation in the absence or presence of SOS. The Tyr402 sidechain in the NMR structure of FH7$_{402H}$, also adopted this conformation. These observations strongly imply that the NMR structure of FH7$_{402H}$, together with the crystal structure of FH678$_{402H}$, provide an excellent basis upon which to reliably model the structure of the FH678$_{402Y}$ structure, which could not be crystallized.

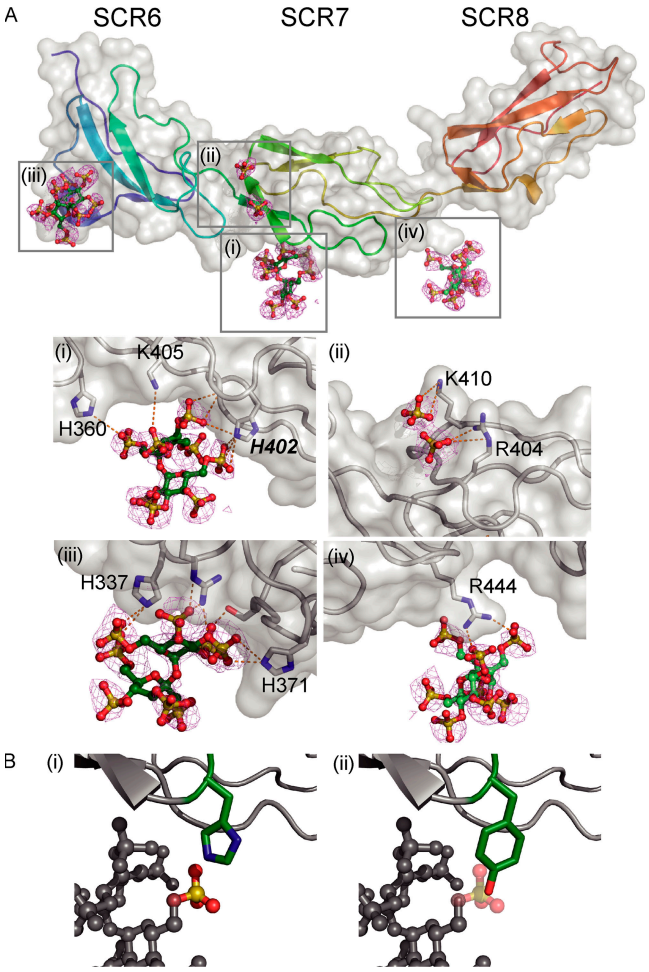

Figure 1. The structure of FH modules 6–8 reveals multiple sulfated sugar-binding sites. (A) The overall structure of FH678$_{402H}$ is shown in cartoon representation colored from blue at the N terminus (residue 320) to red at the C terminus (residue 506). Electron density for the bound SOS is presented as an F_O–F_C map contoured at 2 σ, which was generated before any modeling of the sugar was attempted. All figures were generated using PyMOL (25). SOS-binding sites are labeled (i–iv) and enlarged views are shown below the main panel. SOS is represented as a ball and stick colored by atom type (C, green; O, red; N, blue; S, yellow). Amino acid sidechains that contact the sugar are shown in stick representation, whereas the rest of the protein molecule is shown as a ribbon. Intermolecular hydrogen bonds are shown as dashed orange lines. The polymorphic residue associated with AMD (His402) is highlighted. (B) Model illustrating the proposed ability of the Tyr/His polymorphism at position 402 to differentially bind sulfated sugars. Position of Tyr402 was taken from the NMR structure of FH7$_{402Y}$ (Protein Data Bank ID, 2JGX).

Direct role for AMD-related polymorphic residue in glycan binding

The crystals of FH678$_{402H}$ contain SOS bound to several distinct sites spanning multiple SCRs (Fig. 1). Significantly,

Table I. Refinement statistics and model quality

Crystal	Native	SeMet 1
Wavelength (Å)	0.978	0.979
Space group (Z)	$C222_1$ (8)	$C222_1$ (8)
Cell parameters (Å)	a = 74.7 b = 92.5 c = 57.3	a = 75.0 b = 92.5 c = 57.1
Resolution range (Å)	15.0–2.35 (2.42–2.35)	15.0–2.50 (2.57–2.50)
Unique reflections	8,366	7,044
R_{work} (%)	0.214 (0.230)	0.217 (0.215)
R_{free} (%)	0.246 (0.280)	0.259 (0.266)
Rmsd bond lengths (Å)	0.013	0.017
Rmsd bond angles (°)	1.26	1.14
Residues modelled	320–506	320–506
Waters modeled	133	81
Mean B (A^2) protein	37.8	40.8
SOS	85.7	80.9
Waters	56.2	51.3
Nonprotein molecules	2 SOS[a] 2 Chloride 3 Sulfate 1 Acetate	1 SOS[a] 2 Chloride 3 Sulfate

[a]Crystallographically, there is a single SOS-binding site, but the single site mediates contacts to multiple copies of $FH678_{402H}$ and is filled by two partially occupied molecules in subtly different conformations in the Native crystal form.

the AMD-associated His402 residue in SCR7 is directly hydrogen bonded to a sulfate group of the ligand; His402 and His360 from SCR6 form a histidine clamp around SOS sulfate groups (Fig. 1 A and Fig. S3, available at http://www.jem.org/cgi/content/full/jem.20071069/DC1). The mode of sulfate recognition observed for this ligand is incompatible with the presence of a tyrosine sidechain at position 402, as observed in the previously solved three-dimensional structure of the isolated $FH7_{402Y}$ (Fig. 1 B). This explains the key earlier observations that the His402 and Tyr402 FH variants have altered affinities and specificities for differently sulfated GAGs (18, 19, 21). The rest of this binding site is dominated by hydrogen bonds and Van der Waals contacts with the backbone, with an additional contribution from the more distant positively charged Lys405 (which has been previously implicated in heparin binding by mutagenesis [references 16 and 18]). Significantly, the SOS at this site is present in major and minor conformations in the native protein crystals, related by a rotation of the sulfated fructose ring (Fig. S4 and Supplemental materials and methods). This conformational difference in SOS is accompanied by reorganization of the sidechain of Tyr390 that accommodates one of the repositioned sulfate groups. In the ligand-free form of FH7, only the minor conformation of the tyrosine sidechain is observed (NMR structure of isolated FH7 [reference 19]). A role for Tyr390 in binding heparin is consistent with NMR chemical shift perturbation studies on SCR7 studied in isolation from SCR6 and 8 (19). A secondary SOS-binding site is observed on the opposite face of SCR7. However, ambiguous electron density at this site only allowed modeling of the coordinated sugar sulfates at this site (Fig. 1 A and Supplemental materials and methods). These sulfates contact the Arg404 and Lys410 sidechains, which were previously implicated in heparin binding by mutagenesis (16, 18), and they are also consistent with the NMR chemical shift perturbation studies of isolated FH7 (Fig. 2) (19).

Definition of a novel glycan-binding site in SCR6 and additional sites across SCR7 and 8

Unexpectedly, in addition to the involvement of H360 from SCR6 in the major SCR7-centered binding site, the structure reveals a previously undescribed GAG-binding site contained entirely within SCR6. This third site is chemically similar to that seen in SCR7, with a central positively charged residue (Arg341) flanked by two histidine sidechains (His337 and His371) that directly coordinate two ligand sulfate groups (Fig. 1 and Fig. S1). Analysis of the SOS surface area buried within the two major binding sites in SCR6 and 7, using the program MSDpisa (23), demonstrates that they have similarly sized ligand interfaces (253 and 217 $Å^2$, respectively). Finally, a fourth SOS-binding site in the crystal was observed in the linker between SCR7 and 8; it involves a salt bridge between an SOS sulfate and Arg444.

Mutagenesis and chemical shift perturbations support the hypothesis of extended GAG interactions across the surface of SCR6–8

Previous work has mapped GAG-binding sites on FH to single modules that are spread over the length of FH. In addition to SCR7 (13), the C-terminal module (SCR20) (12)

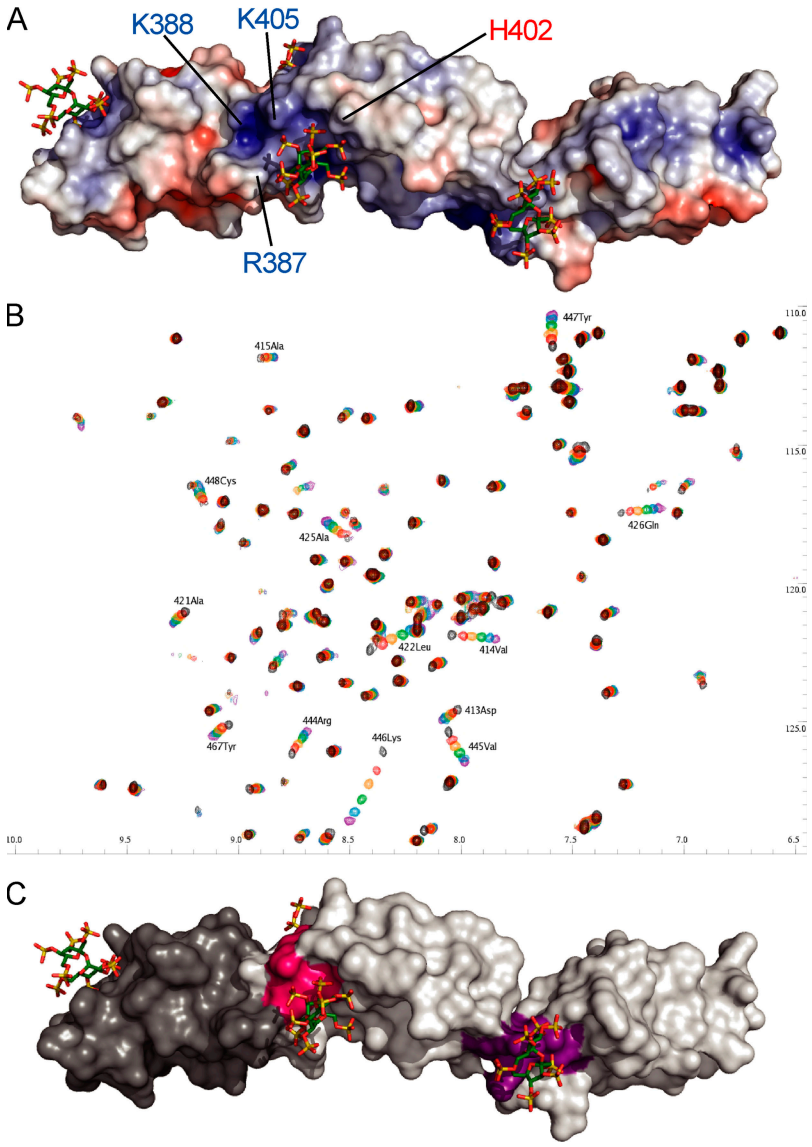

Figure 2. Characterization of GAG-binding sites. (A) Electrostatic surface potential (plotted at ± 5 kT/e) of $FH678_{402H}$ reveals a positively charged groove that extends between the three major SOS-binding sites. The residues lining the groove that have previously associated with polyanion binding, Arg387, Lys388, and Lys405 (16, 18), are highlighted in blue. The polymorphic residue associated with AMD (His402) is highlighted in red (2–5). (B; ^{1}H, ^{15}N) HSQC spectrum for free $FH78_{402Y}$ (50 μM; black) and in the presence of SOS. Protein/ligand ratios are 1:0.6 (red), 1:1.2 (orange), 1:2.5 (green), 1:5 (blue), and 1:10 (purple). The y axis corresponds to ^{15}N chemical shifts, and the x axis corresponds to ^{1}H chemical shifts, both in parts per million. Conditions were 20 mM potassium phosphate, pH 7.4, 298 K. (C) Chemical shift perturbations mapped on the surface of $FH678_{402H}$. SCR6 is shown in dark gray, as it was not present in the constructs used for these experiments. The sidechains of residues that exhibit the largest combined ^{15}N and ^{1}H chemical shift perturbations are highlighted in pink (FH7) and purple (FH78). The data presented in B and C are also shown in Fig. S4 with the molecule rotated in other views. Fig. S4 is available at http://www.jem.org/cgi/content/full/jem.20071069/DC1.

and SCR9 and 13 have been implicated in this respect (15, 24). The electrostatic potential computed from our crystal structure shows that the three GAG-analogue binding sites for which full density could be observed occupy a positively charged groove extending over all three modules of $FH678_{402H}$ (Fig. 2 A and Fig. S5, available at http://www.jem.org/cgi/content/full/jem.20071069/DC1). In addition to the AMD-related polymorphism, which lies at the center of the major binding site in SCR7 within this channel, other residues (Arg387, Lys388, and Lys405) previously implicated in polyanion recognition by mutagenesis (16, 18) also line this groove. Thus, we hypothesize that rather than binding to discrete modules of FH as previously supposed, a GAG molecule on the cell surface can span multiple neighboring modules within the protein. To test this model, and to show that GAG binding is not entirely SCR7 dependent, we performed NMR chemical shift perturbation studies. By titrating either SOS or a highly sulfated heparin tetrasaccharide into ^{15}N-labeled

FH78 (in either allelic form), large chemical shift perturbations were observed for residues 443–447 in the SCR7–8 linker (Fig. 2, B and C, and Fig. S1). This binding site includes the Arg444 seen to contact SOS in the crystal structure (Fig. 1 A). Interestingly, chemical shift perturbations corresponding to the secondary SOS-binding site in SCR7 (Arg404/Lys410), which was observed in NMR studies of SCR7 alone (19), are no longer observed in the context of FH78, suggesting that the FH78 linker site outcompetes the Arg404/Lys410 site. No appreciable chemical shift perturbations were detected for His402, implying the major SCR7-binding site observed in the crystal is not occupied in the absence of the contribution of His360 from SCR6.

To further validate the multiple GAG-binding sites, we generated three domain-deletion FH constructs (FH56, $FH67_{402H}$, and $FH78_{402H}$) and mutated residues within the newly identified SCR6 GAG-binding site. GAG-binding was assayed using heparin-affinity chromatography (Fig. 3, A and B, and Fig. S6, available at http://www.jem.org/cgi/content/full/jem.20071069/DC1). FH56, which completely lacks the previously defined GAG-binding site in SCR7, specifically binds to a heparin-affinity column, demonstrating binding by the SCR6 site in the absence of the SCR7-centered site. The presence of SCR8 greatly increases the affinity of the FH constructs for heparin, which is in agreement with the NMR studies. The contributions made by the various binding sites to heparin binding are further demonstrated by analysis of the pH dependency of the deletion constructs. FH56 and $FH67_{402H}$ bind with a higher affinity at a more acidic pH, presumably caused by increasing protonation of the His residues that dominate the binding sites in SCR6 and 7. Binding of $FH78_{402H}$ on the other hand, is not pH-dependent in the physiological range, confirming the dominance of Arg/Lys residues in the binding site at the SCR7–8 linker. To further probe the novel GAG-binding site in SCR6, point mutations were made in the $FH67_{402H}$ construct, and heparin-binding was assessed (Fig. 3 B). Mutation of either His337 or Arg341 to Ala reduces the affinity of $FH67_{402H}$ for heparin relative to the native $FH67_{402H}$, proving a role for these residues in GAG binding.

Implications for natural function and the disease state

The crystal structure and supporting characterization we present in this study formally demonstrate the presence of multiple GAG-binding sites in FH SCR6–8, which is consistent with a single bound GAG molecule spanning all three modules (Fig. S5). As a further test of this hypothesis, we have also performed an analytical ultracentrifugation analysis of a mixture of extended heparins (dp18 or dp24, selected to be long enough to bridge between the SCR6 and 8 binding sites) and FH678. This analysis (Fig. S7 and Table S1, available at http://www.jem.org/cgi/content/full/jem.20071069/DC1) reveals that the complex formed, with both variants, has a stoichiometry of 1 FH678:1 heparin molecule, as predicted

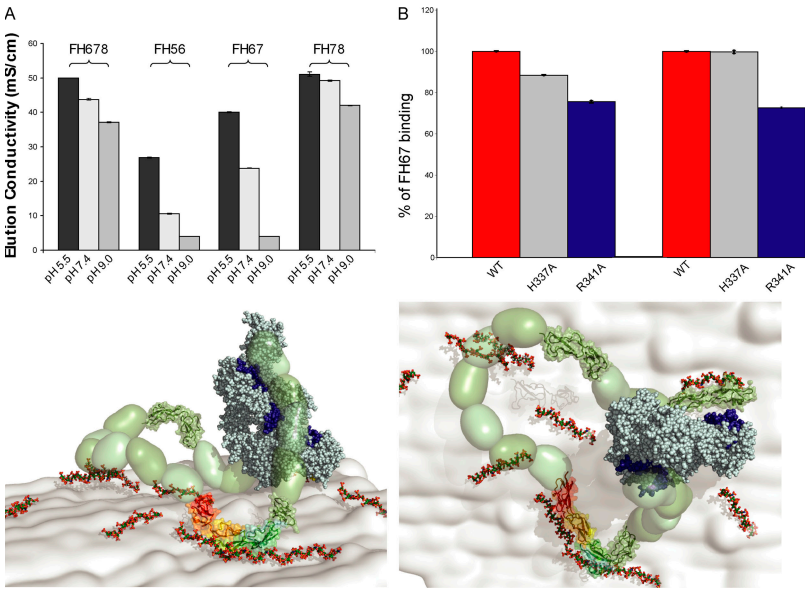

Figure 3. Proposed model for FH interactions with sulfate-rich domains of GAGs on the cell surface. (A) Analysis of binding of different fragments of FH_{402H} to a heparin-HiTrap column confirms the binding site in SCR6 and reveals pH dependency of binding by SCR6 and 7. This supports the involvement of histidine sidechains in glycan coordination, as revealed by the structure. (B) Mutation of sidechains seen to coordinate SOS in SCR6 alter the affinity of $FH67_{402H}$ for a heparin-HiTrap column. (C and D) Model for simultaneous FH binding to C3b (light blue spheres; PDB code, 2I07 [reference 26]) and GAGs (red/green spheres; PDB code, 1HPN [reference 27]) on the retinal epithelium. FH modules for which structural data is available are represented as cartoons and semitransparent surfaces: SCR5 (28), SCR6–8 (PDB code 2UWN; this study), SCR15/16 (Protein Data Bank ID, 1HFH [reference 29]), SCR19/20 (PDB code 2G7I/2BZM [references 30, 31]). Mutational data (dark blue spheres; for review see [reference 32]) mapped onto the structure of C3b suggest FH coils around C3b like a snake.

by our hypothesis of extended interactions with long GAGs. Therefore, we propose a model by which GAG binding to all three modules acts in tandem with binding to SCR20 to localize FH to surface and simultaneously grasp C3b in a pincer grip, accelerating the decay of the C3 convertase assembly and promoting recruitment of factor I (Fig. 3, C and D). We also demonstrate that the polymorphic AMD-associated residue is directly involved in this binding. Switching between histidine and tyrosine at position 402 of FH will alter the mode of GAG binding by changing the specificity for particular sulfation patterns (Fig. 1 B), as previously observed experimentally (18). This ability of FH to register the presence or absence of a single, specific sulfate group within the context of a longer GAG is shown to be dependent on which amino acid residue occupies position 402. Such a subtle effect of the SCR 7 polymorphism is entirely consistent with the obvious fact that either allotype functions adequately in the majority of tissue contexts, and even in the macula until old age. In combination with age-related alterations of retinal GAG composition (17), differences in tissue localization and retention of the polymorphic forms of FH would become significant in the retina over the decades taken for AMD to develop.

MATERIALS AND METHODS

Structure determination. Crystallization trials with both allelic forms, with and without sugar ligand (SOS) were performed as previously described (22); however, only the combination of the H402 construct with a 10-fold excess of SOS yielded crystals. Having obtained crystals, the structure was solved using a combination of molecular replacement (with the NMR structure for SCR7 [reference 19]) and experimental phases from selenomethionine-labeled crystals and Br and Cl heavy atom soaks. Data and coordinates have been deposited in the Protein Data Bank with identifiers 2UWN and 2V8E.

Ligand fitting. SOS was autofit into the major residual electron density in the native data, placing the glucose ring in density, followed by manual rotation around the glycosidic bond to place the fructose ring in density. When repeated in the SeMet-1 density, the SOS was placed in an alternate conformation. Refinement of the occupancies of these alternate conformations led to a model for the native crystals containing SOS conformations 1 and 2 at a ratio of 0.35:0.4, whereas the SeMet-1 crystal only contains conformation 2 (presumably a consequence of SeMet residues in the immediate vicinity of the SOS-binding site). A secondary SOS-binding site was identified on another face of FH-678_{402H} on a crystallographic twofold down the y axis. Attempts to fit an asymmetric SOS into the symmetric residual density were not satisfactory; therefore, only the major density residuals with a tetrahedral shape were modeled with sulfate molecules.

Generation of two-domain constructs and site-directed mutants. The primers used are detailed in the Supplemental materials and methods. Two-domain constructs were amplified and ligated into a pET-14b expression vector (Novagen), via a pDrive cloning vector (Qiagen). Mutations in the SCR6 heparin-binding site were generated in construct FH-67 using the QuikChange site-directed mutagenesis kit (Stratagene). All recombinant proteins were expressed in *Escherichia coli* BL21 (DE3; Novagen) and refolded from inclusion bodies, as previously described (22).

Heparin-binding assays. The relative affinities of the FH fragments for heparin were assayed as the conductivity (milliSiemen/centimeter) required to elute the protein from a 1-ml HiTrap heparin affinity column (GE Healthcare). The purified FH fragments were dialyzed into loading buffer (buffer A) before being injected onto the preequilibrated column. After washing to remove any unbound sample, a gradient of buffer B, ranging from 0–100% over 20 column volumes, was started. The buffers used are described in the Supplemental materials and methods. The point of protein elution is read as the conductivity at which the UV absorbance shows protein elution to be at a maximum. Each experiment was repeated a minimum of five times.

Chemical shift perturbation experiments. FH78 was expressed and purified as previously described (19). NMR spectra were acquired on an AVANCE 600-MHz spectrometer (Bruker) using 5-mm probes. Data for backbone assignment of FH78 were acquired at 310 K on a 0.8-mM sample of ^{13}C, ^{15}N–labeled protein in 20 mM sodium acetate, pH 5.2. Subsequent transfer of the backbone NH assignment to the SOS titration conditions (50 μM protein, 298 K, and 20 mM potassium phosphate, pH 7.4) was achieved with the help of pH and temperature titrations.

Analytical ultracentrifugation. Sedimentation equilibrium experiments to determine the molecular mass of FH678 (both variants) in the presence and absence of a twofold excess of either dp18 or dp26 heparin were performed as described in the Supplemental materials and methods.

Online supplemental material. Fig. S1 shows a NMR titration histogram. Fig. S2 shows a comparison of the binding of histidine and tyrosine FH variants to differently sulfated heparin preparations. Fig. S3 shows an analysis of the major binding sites in SCR6 and SCR7. Fig. S4 shows the effects of ligand binding on Tyr390. Fig. S5 shows the mapping of major features onto the surface of FH-678_{402H}. Fig. S6 is an example of an elution profile from heparin column. Fig. S7 is an AUC experiment. Table S1 lists the molecular weight estimates from sedimentation equilibrium experiments in the presence or absence of heparin dp18 or dp26. A Supplemental materials and methods is also provided. The online version of this article is available at http://www.jem.org/cgi/content/full/jem.20071069/DC1.

We thank Gérard Bricogne and Global Phasing for access to a beta version of Buster-TNT. We are grateful to the staff at the European Synchrotron Radiation Facility protein crystallography beamlines and to Martin Noble, Ed Lowe, and other members of the Laboratory of Molecular Biophysics at the University of Oxford for assistance with data collection. Analytical ultracentrifugation experiments were conducted at the Biomolecular Analysis core facility, Faculty of Life Sciences, University of Manchester.

B. Prosser is funded by the Wellcome Trust Structural Biology Training Program (075415/Z/04/Z). S. Johnson and P. Roversi were funded by grants to S.M. Lea from the Medical Research Council (MRC) of the United Kingdom (grants G0400389 and G0400775). D. Uhrin and P.N. Barlow were funded by the Wellcome Trust (078780/Z/05/Z). S.J. Clark was funded by an MRC Doctoral Training Account (G78/7925), and R.B. Sim and A.J. Day were funded by MRC core funding to the MRC Immunochemistry Unit.

We have no further conflicting financial interests.

Submitted: 25 May 2007
Accepted: 31 August 2007

REFERENCES

1. Friedman, D.S., B.J. O'Colmain, B. Munoz, S.C. Tomany, C. McCarty, P.T. de Jong, B. Nemesure, P. Mitchell, and J. Kempen. 2004. Prevalence of age-related macular degeneration in the United States. *Arch. Ophthalmol.* 122:564–572.
2. Klein, R.J., C. Zeiss, E.Y. Chew, J.Y. Tsai, R.S. Sackler, C. Haynes, A.K. Henning, J.P. SanGiovanni, S.M. Mane, S.T. Mayne, et al. 2005. Complement factor H polymorphism in age-related macular degeneration. *Science.* 308:385–389.
3. Haines, J.L., M.A. Hauser, S. Schmidt, W.K. Scott, L.M. Olson, P. Gallins, K.L. Spencer, S.Y. Kwan, M. Noureddine, J.R. Gilbert, et al. 2005. Complement factor H variant increases the risk of age-related macular degeneration. *Science.* 308:419–421.

4. Edwards, A.O., R. Ritter III, K.J. Abel, A. Manning, C. Panhuysen, and L.A. Farrer. 2005. Complement factor H polymorphism and age-related macular degeneration. *Science*. 308:421–424.
5. Hageman, G.S., D.H. Anderson, L.V. Johnson, L.S. Hancox, A.J. Taiber, L.I. Hardisty, J.L. Hageman, H.A. Stockman, J.D. Borchardt, K.M. Gehrs, et al. 2005. A common haplotype in the complement regulatory gene factor H (HF1/CFH) predisposes individuals to age-related macular degeneration. *Proc. Natl. Acad. Sci. USA*. 102:7227–7232.
6. Day, A.J., A.C. Willis, J. Ripoche, and R.B. Sim. 1988. Sequence polymorphism of human complement factor H. *Immunogenetics*. 27: 211–214.
7. Ripoche, J., A.J. Day, T.J. Harris, and R.B. Sim. 1988. The complete amino acid sequence of human complement factor H. *Biochem. J.* 249:593–602.
8. Kazatchkine, M.D., D.T. Fearon, and K.F. Austen. 1979. Human alternative complement pathway: membrane-associated sialic acid regulates the competition between B and beta1 H for cell-bound C3b. *J. Immunol.* 122:75–81.
9. Weiler, J.M., M.R. Daha, K.F. Austen, and D.T. Fearon. 1976. Control of the amplification convertase of complement by the plasma protein beta1H. *Proc. Natl. Acad. Sci. USA*. 73:3268–3272.
10. Whaley, K., and S. Ruddy. 1976. Modulation of the alternative complement pathways by β1H globulin. *J. Exp. Med.* 144:1147–1163.
11. Fearon, D.T. 1978. Regulation by membrane sialic acid of beta1H-dependent decay-dissociation of amplification C3 convertase of the alternative complement pathway. *Proc. Natl. Acad. Sci. USA*. 75:1971–1975.
12. Blackmore, T.K., J. Hellwage, T.A. Sadlon, N. Higgs, P.F. Zipfel, H.M. Ward, and D.L. Gordon. 1998. Identification of the second heparin-binding domain in human complement factor H. *J. Immunol.* 160:3342–3348.
13. Blackmore, T.K., T.A. Sadlon, H.M. Ward, D.M. Lublin, and D.L. Gordon. 1996. Identification of a heparin binding domain in the seventh short consensus repeat of complement factor H. *J. Immunol.* 157:5422–5427.
14. Pangburn, M.K., M.A. Atkinson, and S. Meri. 1991. Localization of the heparin-binding site on complement factor H. *J. Biol. Chem.* 266: 16847–16853.
15. Ormsby, R.J., T.S. Jokiranta, T.G. Duthy, K.M. Griggs, T.A. Sadlon, E. Giannakis, and D.L. Gordon. 2006. Localization of the third heparin-binding site in the human complement regulator factor H1. *Mol. Immunol.* 43:1624–1632.
16. Giannakis, E., T.S. Jokiranta, D.A. Male, S. Ranganathan, R.J. Ormsby, V.A. Fischetti, C. Mold, and D.L. Gordon. 2003. A common site within factor H SCR 7 responsible for binding heparin, C-reactive protein and streptococcal M protein. *Eur. J. Immunol.* 33:962–969.
17. Verdugo, M.E., and J. Ray. 1997. Age-related increase in activity of specific lysosomal enzymes in the human retinal pigment epithelium. *Exp. Eye Res.* 65:231–240.
18. Clark, S.J., V.A. Higman, B. Mulloy, S.J. Perkins, S.M. Lea, R.B. Sim, and A.J. Day. 2006. His-384 allotypic variant of factor H associated with age-related macular degeneration has different heparin binding properties from the non-disease-associated form. *J. Biol. Chem.* 281: 24713–24720.
19. Herbert, A.P., J.A. Deakin, C.Q. Schmidt, B.S. Blaum, C. Egan, V.P. Ferreira, M.K. Pangburn, M. Lyon, D. Uhrin, and P.N. Barlow. 2007. Structure shows glycosaminoglycan- and protein-recognition site in factor H is perturbed by age-related macular degeneration-linked SNP. *J. Biol. Chem.* 282:18960–18968.
20. Sjoberg, A.P., L.A. Trouw, S.J. Clark, J. Sjolander, D. Heinegard, R.B. Sim, A.J. Day, and A.M. Blom. 2007. The factor H variant associated with age-related macular degeneration (His-384) and the non-disease-associated form bind differentially to C-reactive protein, fibromodulin, DNA, and necrotic cells. *J. Biol. Chem.* 282:10894–10900.
21. Skerka, C., N. Lauer, A.A. Weinberger, C.N. Keilhauer, J. Suhnel, R. Smith, U. Schlotzer-Schrehardt, L. Fritsche, S. Heinen, A. Hartmann, et al. 2007. Defective complement control of Factor H (Y402H) and FHL-1 in age-related macular degeneration. *Mol. Immunol.* 44:3398–3406.
22. Prosser, B.E., S. Johnson, P. Roversi, S.J. Clark, E. Tarelli, R.B. Sim, A.J. Day, and S.M. Lea. 2007. Expression, purification, cocrystallisation and preliminary crystallographic analysis of sucrose octasulfate/human complement regulator factor H SCRs 6-8. *Acta Crystallogr.* F63:480–483.
23. Krissinel, E., and K. Henrick. 2005. Detection of protein assemblies in crystals. *In* Lecture Notes in Computer Science. M.R. Berthold, editor. Springer, Berlin/Heidelberg. 163–174 pp.
24. Pangburn, M.K., M.A. Atkinson, and S. Meri. 1991. Localization of the heparin-binding site on complement factor H. *J. Biol. Chem.* 266: 16847–16853.
25. DeLano, W.L. 2002. The PyMOL Molecular Graphics System. http://www.pymol.org
26. Janssen, B.J., and P. Gros. 2006. Conformational complexity of complement component C3. *Adv. Exp. Med. Biol.* 586:291–312.
27. Mulloy, B., M.J. Forster, C. Jones, and D.B. Davies. 1993. N.M.R., and molecular-modelling studies of the solution conformation of heparin. *Biochem. J.* 293:849–858.
28. Barlow, P.N., D.G. Norman, A. Steinkasserer, T.J. Horne, J. Pearce, P.C. Driscoll, R.B. Sim, and I.D. Campbell. 1992. Solution structure of the fifth repeat of factor H: a second example of the complement control protein module. *Biochemistry*. 31:3626–3634.
29. Barlow, P.N., A. Steinkasserer, D.G. Norman, B. Kieffer, A.P. Wiles, R.B. Sim, and I.D. Campbell. 1993. Solution structure of a pair of complement modules by nuclear magnetic resonance. *J. Mol. Biol.* 232:268–284.
30. Herbert, A.P., D. Uhrin, M. Lyon, M.K. Pangburn, and P.N. Barlow. 2006. Disease-associated sequence variations congregate in a polyanion recognition patch on human factor H revealed in three-dimensional structure. *J. Biol. Chem.* 281:16512–16520.
31. Jokiranta, T.S., V.-P. Jaakola, M.J. Lehtinen, M. Pärepalo, S. Meri, and A. Goldman. 2006. Structure of complement factor H carboxyl-terminus reveals molecular basis of atypical haemolytic uremic syndrome. *EMBO J.* 25:1784–1794.
32. Janssen, B.J., and P. Gros. 2007. Structural insights into the central complement component C3. *Mol. Immunol.* 44:3–10.